Hindawi
Advances in Condensed Matter Physics
Volume 2022, Article ID 4317275, 11 pages
https://doi.org/10.1155/2022/4317275

*Research Article*

# Single-Phase Silicate Phosphors ($Ba_{1.3}Ca_{0.7-x}SiO_4$:$xDy^{3+}$) Doped with Dysprosium for White Solid-State Lighting

**Desta R. Golja**,[1,2] **Francis B. Dejene**,[3] **and Jung Yong Kim**[4,5]

[1]*Department of Materials Science and Engineering, Jimma Institute of Technology, Jimma University, P.O. Box 378, Jimma, Ethiopia*
[2]*Department of Physics, University of the Free State (QwaQwa Campus), P.O. Box 339, Bloemfontein, South Africa*
[3]*Department of Chemical and Physical Sciences, Walter Sisulu University (Mthatha Campus), Private Bag XI UNITRA 5117, Mthatha, South Africa*
[4]*Department of Materials Science and Engineering, Adama Science and Technology University, P.O. Box 1888, Adama, Ethiopia*
[5]*Center of Advanced Materials Science and Engineering, Adama Science and Technology University, P.O. Box 1888, Adama, Ethiopia*

Correspondence should be addressed to Jung Yong Kim; jungyong.kim@astu.edu.et

Received 10 April 2022; Revised 8 May 2022; Accepted 10 May 2022; Published 24 May 2022

Academic Editor: Da-Ren Hang



Single-phase phosphors have potential advantages such as simple processability, competitive cost, and other optical and optoelectronic properties. Hence, in this study, the silicate phosphors ($Ba_{1.3}Ca_{0.7-x}SiO_4$:$xDy^{3+}$) doped with $Dy^{3+}$ ions ($x = 0.01$–$0.05$) were synthesized and characterized in detail. X-ray diffraction patterns showed that all the silicate phosphors have a $\tau$-phase hexagonal unit cell independent of doping. However, $d$-spacing was reduced for the doped samples, indicating that the interplanar interactions were enhanced. Resultantly, the doped phosphors exhibited relatively larger domains with connectivity than the host, although there were sometimes microscale pores. Photoluminescence spectra stipulated that the optimized doping concentration is $x = 0.03$ for the silicate $Ba_{1.3}Ca_{0.7-x}SiO_4$:$xDy^{3+}$ phosphors. Finally, the CIE coordinates (0.30, 0.33) confirm that the $Dy^{3+}$-doped silicate phosphors are well applicable to the white light-emitting diodes for solid-state lighting and display devices.

## 1. Introduction

The light-emitting diode (LED)-based solid-state lighting (SSL) is relatively a green technology by replacing the conventional incandescent and fluorescence lamps requiring a large amount of energy consumption [1–4]. Therefore, since the Nichia Corporation invented a blue indium-gallium-nitride (InGaN) LED chip coated with a yellow phosphor ($Y_3Al_5O_{12}$:$Ce^{3+}$, YAG: $Ce^{3+}$) in 1996, the phosphor-converted white LED (pc-WLED) has received a surge of global interests due to their high luminous efficacy, stability/reliability, competitive cost, eco-friendliness, and low power consumption [5–7]. However, the low color-rendering index (CRI) and high correlated color temperature are common drawbacks to this kind of LED [8, 9]. Hence, to overcome this limitation, the ultraviolet (UV) LED chips coated with red-green-blue (RGB) trichromatic phosphors were introduced, resulting in high CRI with a partial sacrifice in their quantum efficiencies [10, 11]. However, there are still some technical challenges such as the reabsorption of blue light by the green and red phosphors and the complicated mixing process of these RGB phosphors with a specific ratio for a desirable color balance [12–16].

Meanwhile, the single-phase pc-WLED has been proposed as an alternative to the aforementioned UV-LED with yellow or RGB phosphors [17–28]. Here, the single host matrix (e.g., aluminate, borate, carbonate, fluoride, molybdate, niobate, nitride, phosphate, silicate, tantalite, titanate, and tungstate) was doped with rare earth element (REE) ions (e.g., scandium, yttrium, and other lanthanides) and/or transition metal ions [3, 29]. Here, if the process of doping in luminescent semiconductors is more simplified by

using a single dopant instead of two or three ones, it will be clearly advantageous because both time and cost are saved. Therefore, it should be necessary to study the single-phase single-doped phosphor materials. For this purpose, the trivalent dysprosium ion ($Dy^{3+}$) should be a good activator because it has two main emissions through the magnetic dipole transition at 482 nm (blue: $^4F_{9/2} \longrightarrow {}^6H_{15/2}$) and the electric dipole transition at 577 nm (yellow: $^4F_{9/2} \longrightarrow {}^6H_{13/2}$) [17–28]. Herein, the yellow-emitting process is hypersensitive to the local environment, indicating the luminous intensity is adjustable by modulating the crystal field. As a host material, the silicate phosphors are promising because it has chemical and thermal stabilities [30, 31]. Hence, to date, the versatile silicate phosphors have been examined for pc-WLEDs, which includes $Ca_3Si_2O_7$, $Ca_2Al_2SiO_7$, $Sr_2MgSi_2O_7$, $Ca_2MgSi_2O_7$, $Ca_3MgSi_2O_8$, $K_4CaSi_3O_9$, $BaCa_2Si_3O_9$, $KBaScSi_3O_9$, $Ca_9La(PO_4)_5(SiO_4)F_2$, and $Ca_9La(PO_4)_5(SiO_4)Cl_2$ [3, 29–34].

In this study, we report the concentration effects on the properties of the unique $\tau$-phase silicate $Ba_{1.3}Ca_{0.7-x}SiO_4$:$xDy^{3+}$ phosphors, showing chemical and structural stabilities. For this purpose, we investigated the structural, morphological, and optical properties of $Ba_{1.3}Ca_{0.7-x}SiO_4$:$xDy^{3+}$ as a function of the activator ($Dy^{3+}$) amounts. Here, the photoluminescence (PL) and CIE chromaticity diagram of the $Ba_{1.3}Ca_{0.7-x}SiO_4$:$xDy^{3+}$ samples were of special interests for the single-phase pc-WLED applications.

## 2. Experimental

*2.1. Synthesis of $Ba_{1.3}Ca_{0.7-x}SiO_4$:$xDy^{3+}$.* The single-phase silicate ($Ba_{1.3}Ca_{0.7-x}SiO_4$:$xDy^{3+}$) phosphors were prepared with varying the doping concentration of $Dy^{3+}$ ions ($x = 0.00$, 0.01, 0.02, 0.03, 0.04, and 0.05). Calcium nitrate ($Ca(NO_3)_2 4H_2O$ (99.9%)), barium nitrate ($Ba(NO_3)_2$ (99.9%)), dysprosium(III) nitrate ($Dy(NO_3)_3$ (99.9%)), urea ($CH_4N_2O$ (99.9%)), and tetraethyl orthosilicate (TEOS) (($Si(OC_2H_5)_4$ (99.9%)) were purchased from Sigma-Aldrich and used as received. Stoichiometric amounts of nitrates, TEOS, and urea were dissolved in 10 mL of deionized water [35, 36]. The mixture was constantly stirred at the temperature of 80–90°C, transferred to an alumina crucible, and put into a preheated furnace at 550°C. Then, the solid products ($Ba_{1.3}Ca_{0.7-x}SiO_4$:$xDy^{3+}$) were annealed at 1000°C for 2 h and subsequently crushed for obtaining the fine powder samples.

*2.2. Characterization.* The X-ray diffraction (XRD) pattern data were obtained using the Model Philips Bruker D8 advance. The microstructure of samples was characterized by using the scanning electron microscope (SEM: Model JEOL JSM-7800F). Elemental analysis was carried out using the energy-dispersive X-ray spectroscope (EDS) (Oxford Aztec). Optical bandgap was estimated by using the ultraviolet-visible (UV-Vis) spectrophotometer (Shimadzu evolution 100). The PL data could be obtained by using the Cary Eclipse fluorescence spectrophotometer (model LS-55) equipped with a xenon flash lamp.

## 3. Results and Discussion

*3.1. Structural Analysis.* Figure 1(a) shows the XRD patterns for the prepared silicate phosphors. The diffraction peaks were well indexed with the JCPDS (Joint Committee on Powder Diffraction Standards) card number 36–1449. The silicate phosphors ($Ba_{1.3}Ca_{0.7-x}SiO_4$:$xDy^{3+}$) have the space group ($p\bar{3}m1$) and a hexagonal unit cell [37] with parameters $a = 0.5749$ nm, $c = 1.466$ nm, and volume ($V$) = 0.484 nm$^3$. Figure 1(b) shows the analysis of the most intense (110) peaks. The host material ($Ba_{1.3}Ca_{0.7}SiO_4$) shows the $d$-spacing of 0.291 nm based on Bragg's law $\lambda = 2\ d \sin\ \theta$, where the wavelength of X-ray light ($\lambda$) is 0.154 nm at the diffraction angle $\theta = 15.35°$. On the other hand, the $Dy^{3+}$-doped silicate phosphors ($Ba_{1.3}Ca_{0.7-x}SiO_4$:$xDy^{3+}$ ($x = 0.01$–$0.05$)) display the average $d$-spacing of $0.2888 \pm 0.001$ nm at the angles of $\theta = 15.47°$ ($x = 0.01$), 15.49° ($x = 0.02$), 15.45° ($x = 0.03$), 15.55° ($x = 0.04$), and 15.40° ($x = 0.05$), respectively. This result indicates that when $Dy^{3+}$ ions were incorporated into the host silicate, the interplanar interactions between (110) crystallographic planes were enhanced, resulting in the reduction of $d$-spacing, i.e., the shift of (110) peaks to higher $2\theta$ angles as shown in Figure 1(b). Importantly, it is notable that the ionic radii of $Dy^{3+}$, $Ca^{2+}$, and $Ba^{2+}$ ions are 1.03 Å, 1.06 Å, and 1.34 Å, respectively [38–40], indicating that the dopant $Dy^{3+}$ ions may substitute $Ca^{2+}$ instead of $Ba^{2+}$ ions based on the similarity of ionic sizes [41, 42]. However, uncompensated charges remain in the phosphors due to the aliovalency effect between $Dy^{3+}$ and $Ca^{2+}$ ions, which could be studied as a future work.

The crystallite size ($D_S$) of the phosphor samples can be calculated using Scherrer's equation [43, 44]:

$$D_S = \frac{0.92\lambda}{\beta \cos \theta}, \quad (1)$$

where $\beta$ is the full width at half maximum (FWHM) at the diffraction angle $\theta$, $D_S$ value was estimated to be 29.4 nm for the host sample, whereas the average crystallite size $\overline{D}_S$ for the $Dy^{3+}$-doped silicate phosphors ($x = 0.01$–$0.05$) was $32.8 \pm 5.7$ nm based on the data given in Table 1.

*3.2. Morphological and Elemental Analyses.* Figure 2 shows the SEM images, displaying various morphologies for the silicate powder samples. As shown in Figure 2(a), the host material shows some microscale aggregations of polycrystalline particles. However, when 1 mol% of $Dy^{3+}$ ions was incorporated into the host lattice (i.e., $Ba_{1.3}Ca_{0.7-x}SiO_4$:$xDy^{3+}$ ($x = 0.01$)), the microstructural morphology was changed dramatically, exhibiting relatively uniform domains and their boundaries with good connectivity and aggregation (Figure 2(b)). Note that the $Dy^{3+}$ doping process enhanced the interplanar interactions as confirmed through the XRD data in Figure 1(b). This phenomenon is validated

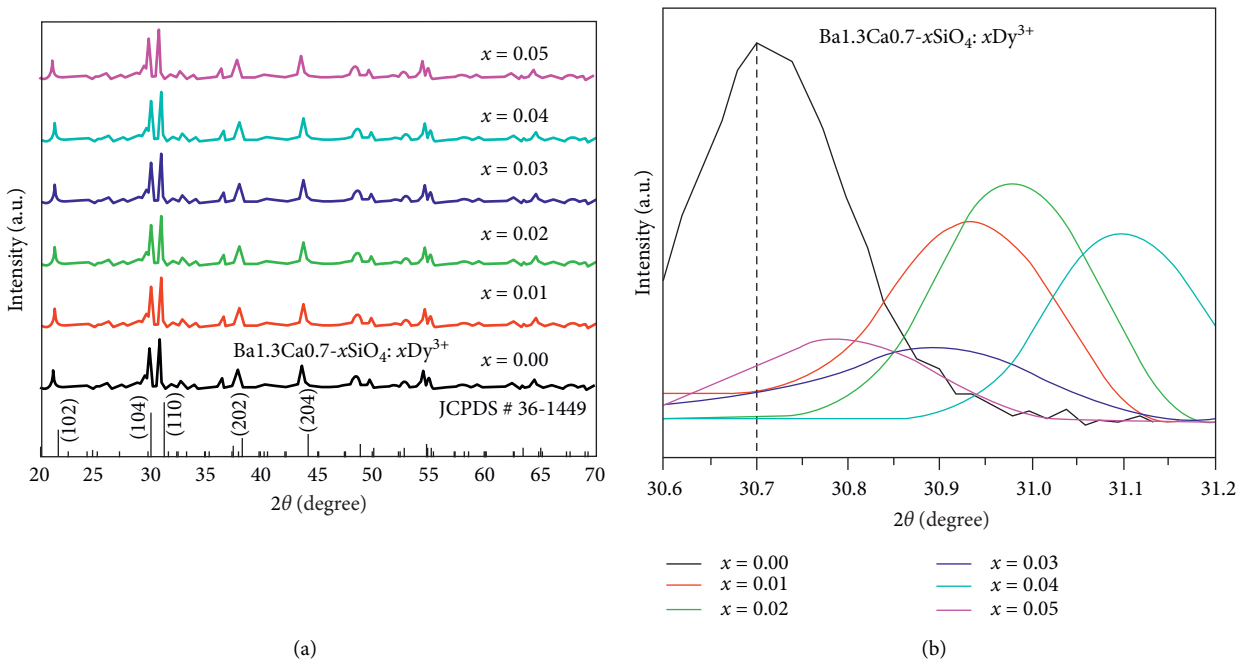


FIGURE 1: (a) XRD patterns of the silicate phosphors, $Ba_{1.3}Ca_{0.7-x}SiO_4{:}xDy^{3+}$ ($x = 0.00$, 0.01, 0.02, 0.03, 0.04, and 0.05). (b) Magnification of the most intense (110) peaks with doping concentration.

TABLE 1: Crystallite size ($D_S$) of the silicate phosphors, $Ba_{1.3}Ca_{0.7-x}SiO_4{:}xDy^{3+}$ ($x = 0.00$, 0.01, 0.02, 0.03, 0.04, and 0.05), as a function of $Dy^{3+}$ doping concentration.

| $Ba_{1.3}Ca_{0.7-x}SiO_4{:}xDy^{3+}$ | $\beta$ (radians) | $\theta$ (°) | $D_S$ (nm) | $d$-spacing (nm) |
|---|---|---|---|---|
| $x = 0.00$ | 0.00366 | 15.35 | 29.4 | 0.2910 |
| $x = 0.01$ | 0.00383 | 15.47 | 36.8 | 0.2889 |
| $x = 0.02$ | 0.00358 | 15.49 | 36.8 | 0.2885 |
| $x = 0.03$ | 0.00520 | 15.45 | 24.5 | 0.2892 |
| $x = 0.04$ | 0.00366 | 15.55 | 36.8 | 0.2874 |
| $x = 0.05$ | 0.00400 | 15.40 | 29.4 | 0.2902 |

The parameter $\beta$ is the FWHM at the diffraction angle $\theta$.

again through the phosphor sample doped with 3–5 mol% (i.e., $x = 0.03$–0.05) of $Dy^{3+}$. Figure 2(c) shows that the sample ($Ba_{1.3}Ca_{0.7-x}SiO_4{:}xDy^{3+}$ ($x = 0.03$)) has the increased aggregation of particles with partial connectivity, but contains significant amounts of micropores, presenting the nonuniform growth process of polycrystalline domains during the rapid gel-combustion reactions in the presence of dopant $Dy^{3+}$ ions. In the same vein, when the doping concentration was increased up to 5 mol % of $Dy^{3+}$ ions ($Ba_{1.3}Ca_{0.7-x}SiO_4{:}xDy^{3+}$ ($x = 0.05$)), the morphology displays an impressive microstructure with relatively large domains and microscale pores, implying the viscous flow in the lateral direction during crystallization and growth of the doped silicate phosphors (Figure 2(d)).

Furthermore, the EDS analysis provides the elemental composition of the silicate phosphor samples. As shown in Figure 3, the host material ($Ba_{1.3}Ca_{0.7}SiO_4$) shows O, Ba, Si, and Ca elements, whereas the $Dy^{3+}$-doped phosphor samples ($Ba_{1.3}Ca_{0.7-x}SiO_4{:}xDy^{3+}$) exhibit the presence of the activator (Dy) in addition to the host components, as given in Table 2.

*3.3. Optical Analysis.* The optical properties of materials are determined by the electronic structure of elements as well as the microstructures (or orbital overlapping) of materials including the shape and size of particles. Figure 4(a) shows the diffuse reflectance spectra of the silicate phosphors, $Ba_{1.3}Ca_{0.7-x}SiO_4{:}xDy^{3+}$ ($x = 0.00$, 0.01, 0.02, 0.03, 0.04, and 0.05), in the range of 250–800 nm. As shown in Figure 4(a), when a sample was doped with $Dy^{3+}$ ions, the reflectance was enhanced. However, depending on the doping concentration, the remission percentage was diversified. For example, when the doping concentration was only 1 mol% of $Dy^{3+}$ ions, the enhanced reflectance was limited in the range of 320–800 nm. On the other hand, when doping was increased more than 2 mol% of $Dy^{3+}$ ions, the reflectance (a backscattering of light) increased in the whole range of

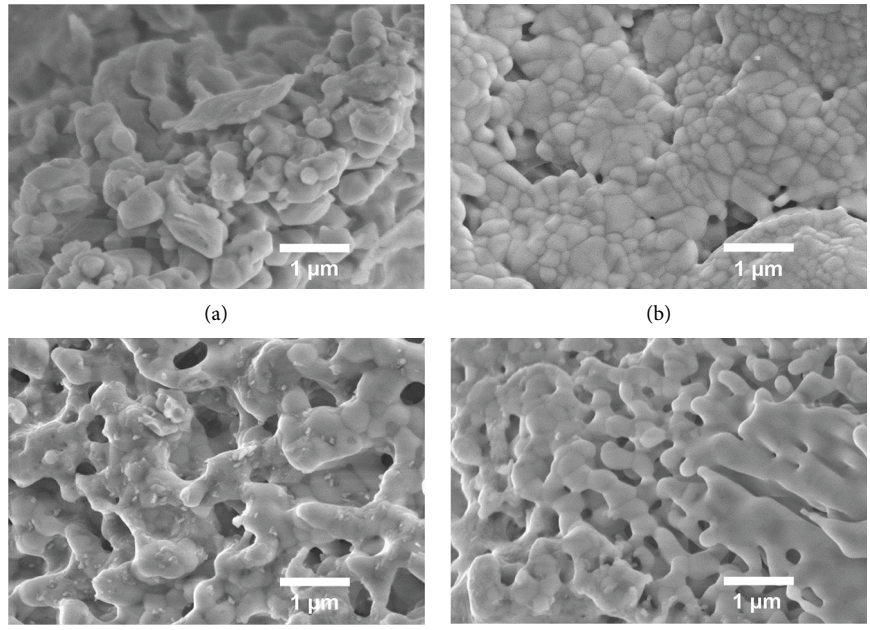


(a) (b) (c) (d)

Figure 2: SEM images of $Ba_{1.3}Ca_{0.7-x}SiO_4{:}xDy^{3+}$: (a) $x = 0.00$, (b) $x = 0.01$, (c) $x = 0.03$, and (d) $x = 0.05$.

Table 2: The weight and atomic percentage of $Ba_{1.3}Ca_{0.7-x}SiO_4{:}xDy^{3+}$ samples as a function of $Dy^{3+}$ doping concentration ($x = 0.00$, 0.01, 0.03, and 0.05) based on the energy-dispersive X-ray spectroscopy (EDS) analysis.

| Phosphor sample | Element | Weight (%) | Atomic (%) |
|---|---|---|---|
| $Ba_{1.3}Ca_{0.7-x}SiO_4{:}xDy^{3+}$ ($x = 0.00$) | Ba | 29.0 | 6.06 |
| | Ca | 16.0 | 11.46 |
| | Si | 21.0 | 21.47 |
| | O | 34.0 | 61.01 |
| $Ba_{1.3}Ca_{0.7-x}SiO_4{:}xDy^{3+}$ ($x = 0.01$) | Ba | 38.7 | 9.48 |
| | Ca | 20.2 | 16.95 |
| | Si | 10.4 | 10.40 |
| | O | 28.9 | 60.75 |
| | Dy | 1.8 | 0.37 |
| $Ba_{1.3}Ca_{0.7-x}SiO_4{:}xDy^{3+}$ ($x = 0.03$) | Ba | 39.6 | 10.21 |
| | Ca | 20.8 | 18.37 |
| | Si | 12.4 | 15.63 |
| | O | 25.0 | 55.31 |
| | Dy | 2.20 | 0.48 |
| $Ba_{1.3}Ca_{0.7-x}SiO_4{:}xDy^{3+}$ ($x = 0.05$) | Ba | 39.6 | 10.51 |
| | Ca | 21.6 | 19.64 |
| | Si | 10.3 | 13.36 |
| | O | 24.4 | 55.57 |
| | Dy | 4.1 | 0.92 |

250–800 nm. Interestingly, when the doping amount was 2 or 5 mol% of $Dy^{3+}$ ions, the reflectance percent was the largest among the samples, indicating that the microstructure including inhomogeneity affect significantly the optical property of materials. Importantly, the prominent absorption band in the range of 300–425 nm should be attributed to the electronic structure (i.e., the transition from ground state of excited one) of $Dy^{3+}$ ions [45, 46].

The Kubelka–Munk (K-M) coefficient was employed to estimate the optical bandgap from the diffuse reflectance spectra [47]:

$$F(R) = \frac{(1-R)^2}{2R}, \tag{2}$$

where $F(R)$ is the K-M function and $R$ is the diffused reflectance. Figure 4(b) shows the plot of "$[F(R) \cdot h\nu]^2$ vs.

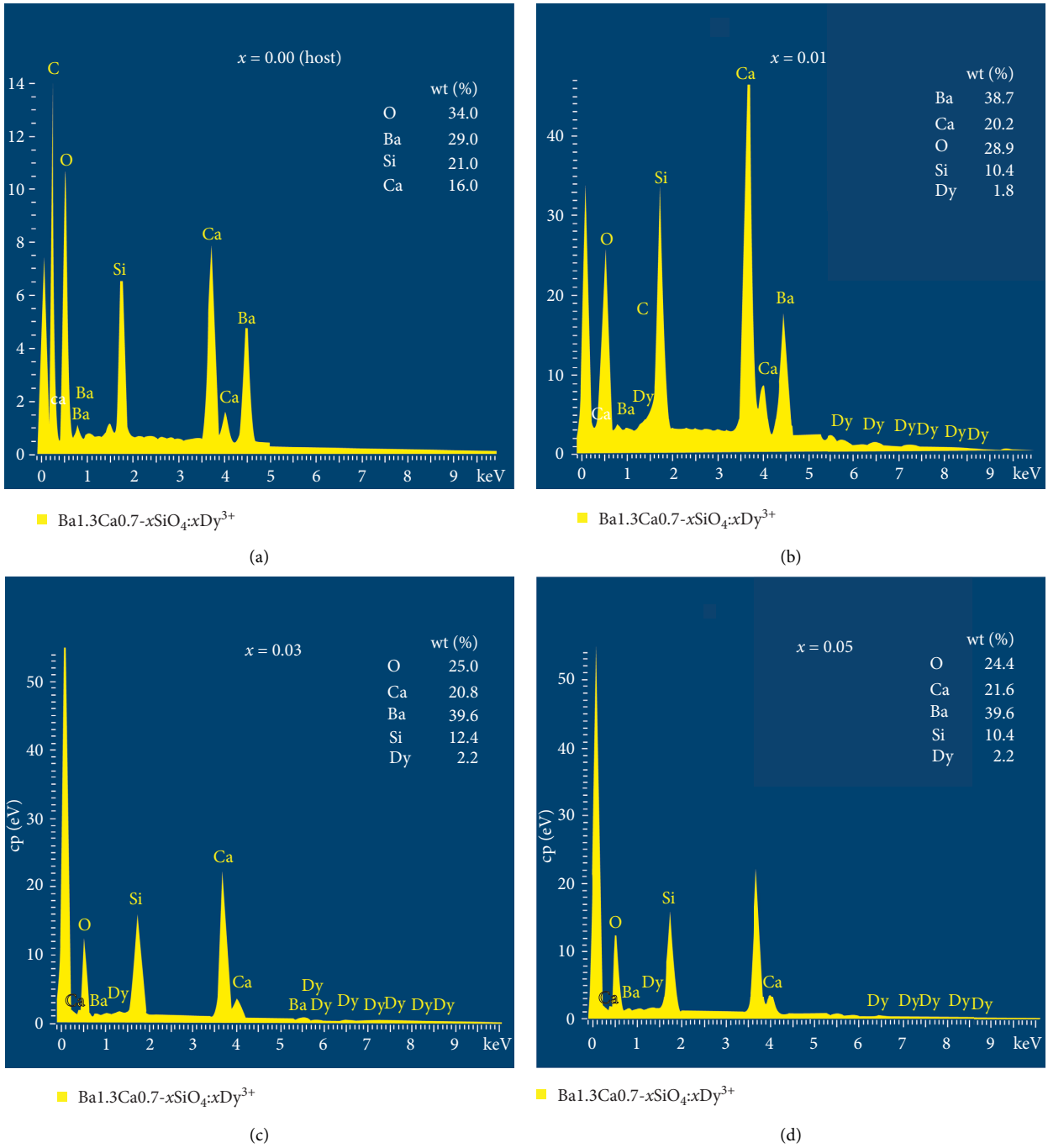


FIGURE 3: EDS spectra for $Ba_{1.3}Ca_{0.7-x}SiO_4{:}xDy^{3+}$: (a) $x = 0.00$, (b) $x = 0.01$, (c) $x = 0.03$, and (d) $x = 0.05$.

photon energy,$h\nu$" for the direct bandgap semiconductor $Ba_{1.3}Ca_{0.7-x}SiO_4{:}xDy^{3+}$ ($x = 0.00$, 0.01, 0.02, 0.03, 0.04, and 0.05), in which $h$ is Planck's constant and $\nu$ is the frequency of a light wave. As shown in Figure 4(b), the bandgap of $Ba_{1.3}Ca_{0.7}SiO_4$ (host) is estimated about 3.85 eV (corresponding to $\lambda$, 33f0 nm), whereas the average bandgap of the doped samples is $3.74 \pm 0.09$ eV (corresponding to $\lambda$, 340 nm). Hence, the doping of $Dy^{3+}$ ions in the silicate host ($Ba_{1.3}Ca_{0.7}SiO_4$) not only brought forth the enhanced interplanar interactions (i.e., a reduced $d$-spacing) but also a red-shift in absorption (i.e., a reduced optical bandgap from 3.85 eV to 3.74 eV). Hence, the UV-vis reflectance and X-ray scattering analyses support each other about the effect of $Dy^{3+}$ doping on the enhanced interplanar interactions of silicate phosphors.

*3.4. Photoluminescence Analysis.* Figure 5(a) shows the PL excitation spectra of $Ba_{1.3}Ca_{0.7-x}SiO_4{:}xDy^{3+}$ as a function of $Dy^{3+}$ concentration, whereas Figure 5(b) is the PL emission spectra showing the most intense peak at 482 nm. Here, in

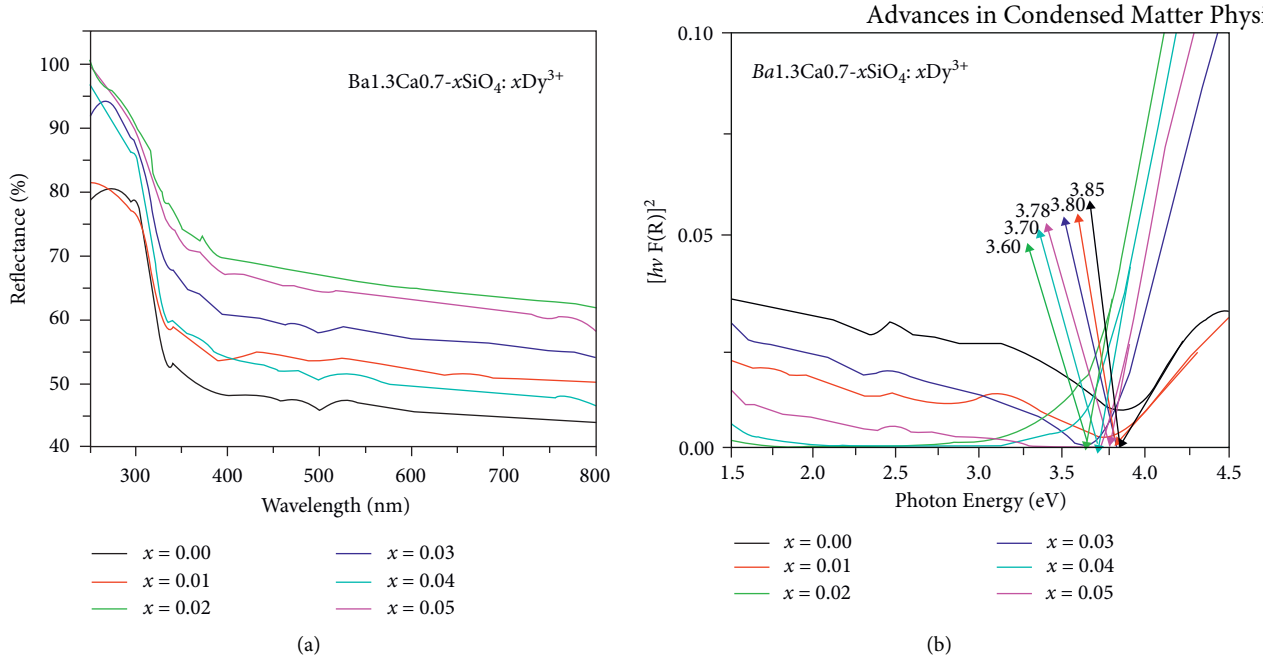


FIGURE 4: (a) UV-Vis diffuse reflectance spectra for $Ba_{1.3}Ca_{0.7-x}SiO_4$:$xDy^{3+}$ ($x = 0.00$, 0.01, 0.02, 0.03, 0.04, and 0.05). (b) Energy bandgap for Ba1.3Ca0.7−xSiO4:$x$Dy3+ ($x = 0.00$, 0.01, 0.02, 0.03, 0.04, and 0.05).

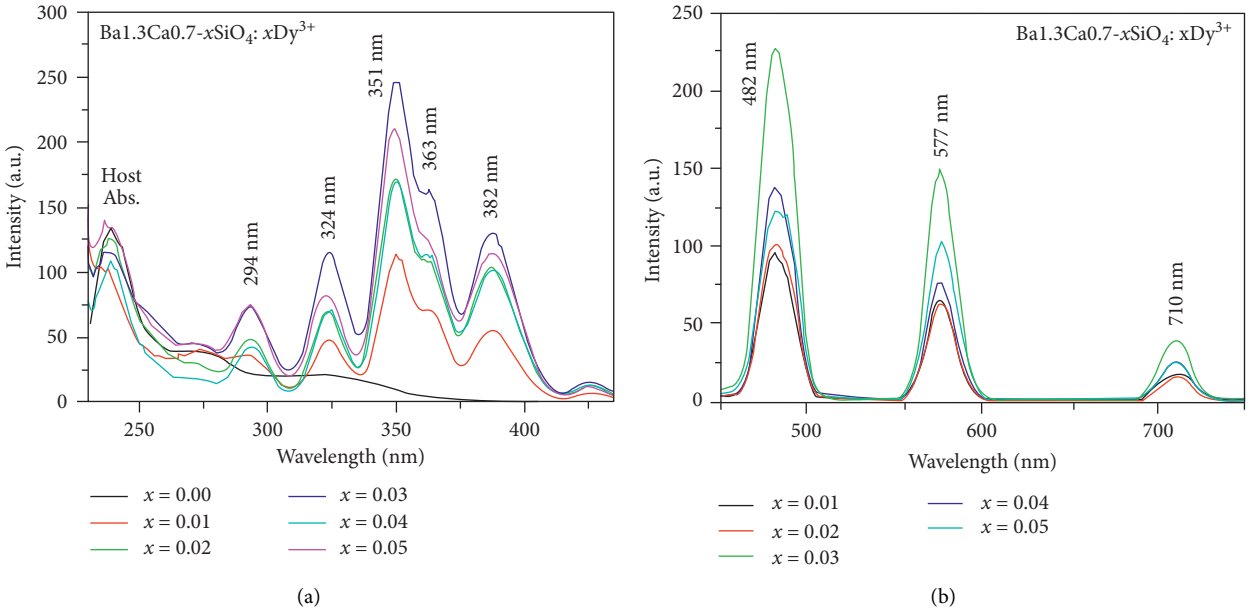


FIGURE 5: Continued.

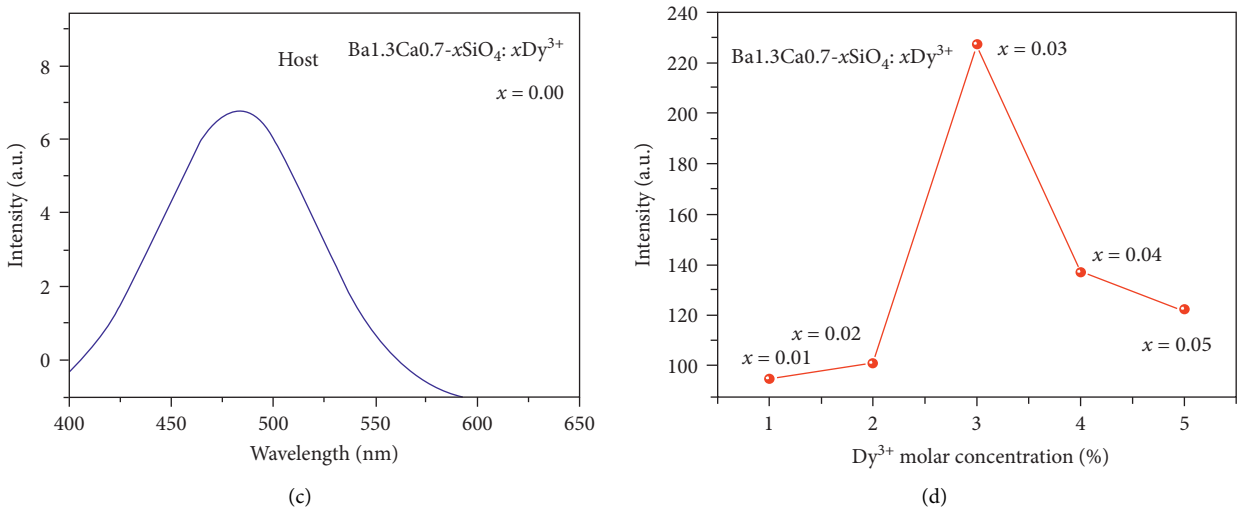


FIGURE 5: (a) Excitation spectra of $Ba_{1.3}Ca_{0.7-x}SiO_4$:$xDy^{3+}$ ($x = 0.01$, 0.02, 0.03, 0.04, and 0.05). (b) Emission spectra of Ba1.3Ca0.7−xSiO4: $x$Dy3+ ($x = 0.01$, 0.02, 0.03, 0.04, and 0.05). (c) Emission spectrum of the host, $Ba_{1.3}Ca_{0.7}SiO_4$. (d) PL intensity as a function of $Dy^{3+}$ molar concentration.

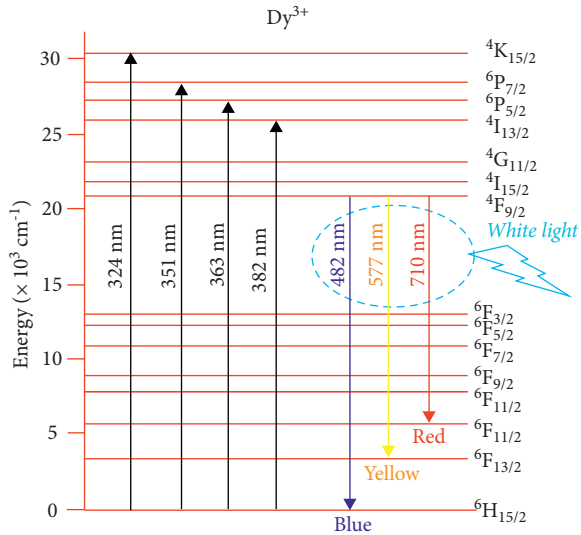


FIGURE 6: Energy level diagram of the activator ($Dy^{3+}$ ions) in the silicate host ($Ba_{1.3}Ca_{0.7}SiO_4$).

the case of the host material, the observed PL may arise from a radiative recombination between electrons and holes trapped in the defect states in the energy bandgap [36]. As shown in Figure 5(a) (specifically, the black solid line), the two weak broad emission bands were observed at 275 and 375 nm, respectively. As shown in Figures 5(a) and 5(b), the PL intensity increases dramatically with increasing the doping concentration of $Dy^{3+}$ ions because the dopant species ($Dy^{3+}$) is a dominant factor for the excitation band of the silicate phosphor materials. In Figure 5(a), all the bands except at 238 nm are assigned to electronic transitions from the ground state $^6H_{15/2}$ to the various excited states in the $4f^9$ orbital configuration of $Dy^{3+}$ ions. Here, the weak PL peak at 238 nm should originate from the host absorption band, whereas that at 294 nm from the $O^{2-} \longrightarrow Dy^{3+}$ transition [24, 48–50]. The other excitation peaks are attributed to the electronic transition $^6H_{15/2} \longrightarrow {}^4K_{15/2}$ at 324 nm, $^6H_{15/2} \longrightarrow {}^6P_{7/2}$ at 351 nm, $^6H_{15/2} \longrightarrow {}^6P_{5/2}$ at 363 nm, and $^6H_{15/2} \longrightarrow {}^4I_{13/2}$ at 382 nm, respectively [51–58]. Figure 5(c) shows the emission spectra of the host material ($Ba_{1.3}Ca_{0.7}SiO_4$) without any dopant, exhibiting a broad emission band at 482 nm from the self-trapped luminescent recombination.

Under the excitation of $\lambda = 351$ nm, the $Dy^{3+}$-doped phosphors ($Ba_{1.3}Ca_{0.7-x}SiO_4$:$xDy^{3+}$) exhibit three emission bands in the range of 450–800 nm with peaks at blue (482 nm), yellow (577 nm), and red (710 nm), which are induced by the $^4F_{9/2} \longrightarrow {}^6H_{15/2}$, $^4F_{9/2} \longrightarrow {}^6H_{13/2}$, and $^4F_{9/}$

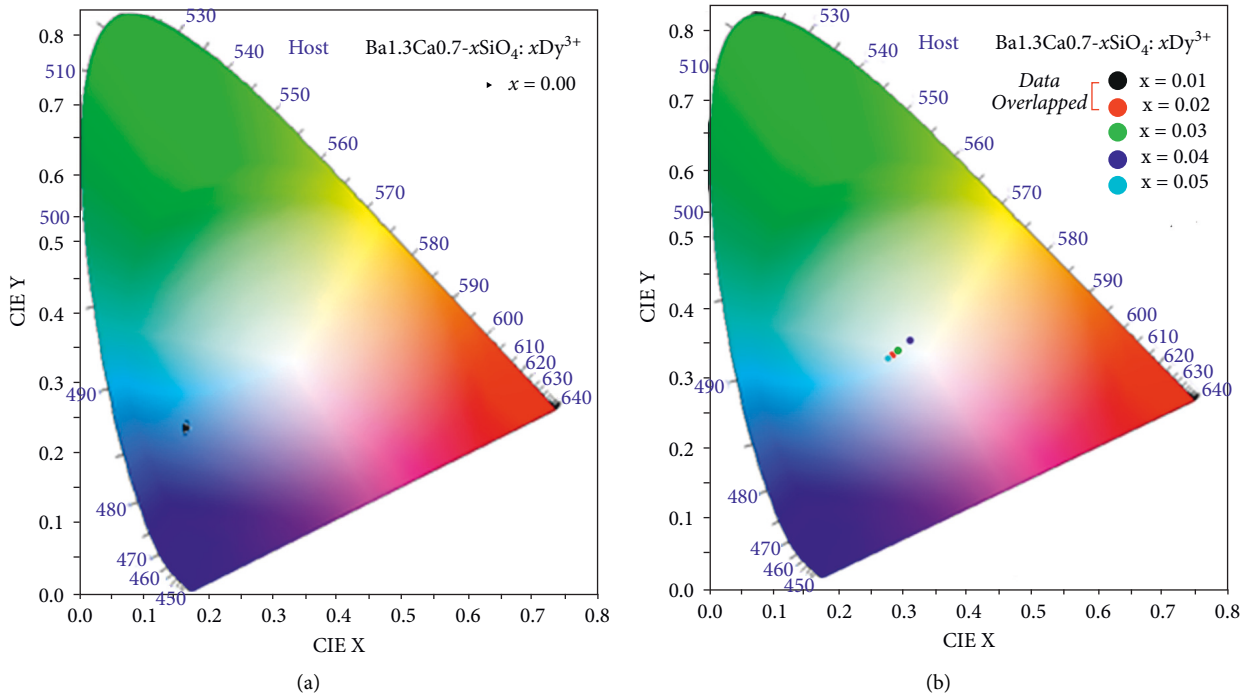


FIGURE 7: CIE chromaticity diagrams for (a) the host $Ba_{1.3}Ca_{0.7-x}SiO_4$:$xDy^{3+}$ ($x = 0.00$) and (b) the doped silicate phosphors, Ba1.3Ca0.7−xSiO4:$xDy^{3+}$ ($x = 0.01$, 0.02, 0.03, 0.04, and 0.05).

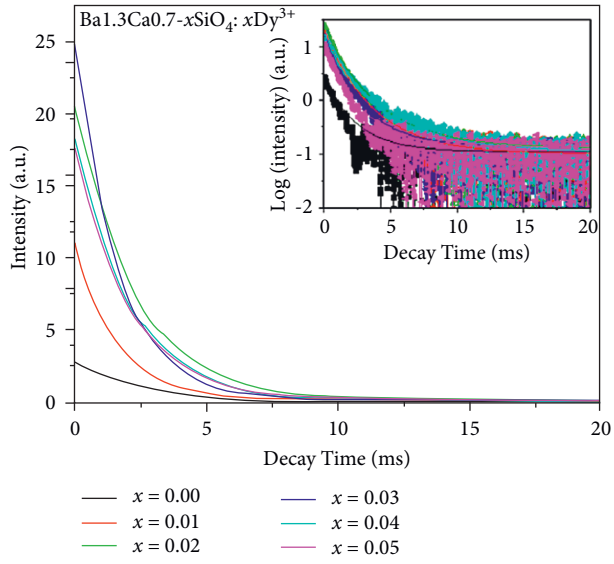


FIGURE 8: PL decay curve for the silicate phosphors, $Ba_{1.3}Ca_{0.7-x}SiO_4$:$xDy^{3+}$ ($x = 0.00$, 0.01, 0.02, 0.03, 0.04, and 0.05). The inset graph shows the plot of "Log (Intensity) vs. Decay Time."

$_2 \longrightarrow {}^6H_{11/2}$ transitions, respectively (Figure 5(b)). Importantly, the blue light emission at 482 nm is ascribed to the magnetic dipole transition, whereas the yellow-light emission at 576 nm is due to electric dipole transition which is known to be hypersensitive and thus strongly influenced by the surrounding environment around the $Dy^{3+}$ ion [52, 53]. Furthermore, according to the Judd-Ofelt theory [54], the electric dipole transition (yellow emission) will be intensified when $Dy^{3+}$ ions are located at low-symmetry sites with no inversion center, whereas the magnetic dipole transition (blue emission) will be strengthened when $Dy^{3+}$ is located at high symmetry with an inversion center. However, the blue emission at 482 nm is usually stronger than the yellow emission, indicating that $Dy^{3+}$ ions occupy a high-symmetry local site with inversion symmetry in this matrix [55]. The intensity of the radiative transition increases with the increase of activator molar concentration from 0 to 3 mol% and then decreases thereafter due to concentration

Table 3: PL decay curve parameters for the silicate phosphors, $Ba_{1.3}Ca_{0.7-x}SiO_4{:}xDy^{3+}$ ($x = 0.00$, 0.01, 0.02, 0.03, 0.04, and 0.05).

| $Ba_{1.3}Ca_{0.7-x}SiO_4{:}xDy^{3+}$ | $A_1$ | $\tau_1$ (ms) | $A_2$ | $\tau_2$ (ms) | $\langle\tau\rangle$ (ms) |
|---|---|---|---|---|---|
| $x = 0.00$ | 22.83 | 0.68 | 2.36 | 2.63 | 1.24 |
| $x = 0.01$ | 2.85 | 2.40 | 18.25 | 0.69 | 1.29 |
| $x = 0.02$ | 15.92 | 0.65 | 2.46 | 2.27 | 1.22 |
| $x = 0.03$ | 0.20 | 4.71 | 2.50 | 0.67 | 2.12 |
| $x = 0.04$ | 4.42 | 2.42 | 13.14 | 0.67 | 1.63 |
| $x = 0.05$ | 0.60 | 3.38 | 10.28 | 0.75 | 1.29 |

quenching (Figure 5(d)). Notably, the hypersensitive transition affords a tunable white color emission by adjusting the ratio of yellow/blue light intensity. Furthermore, the silicate matrix itself should play an important role in this hypersensitive transition because it provides an environment for the activator ions. Resultantly, Figure 6 shows the partial energy level diagram of $Dy^{3+}$ ions in the silicate host, which was constructed based on the excitation and emission spectra of $Ba_{1.3}Ca_{0.7-x}SiO_4{:}xDy^{3+}$ ($x = 0.01$, 0.02, 0.03, 0.04, and 0.05), as shown in Figure 5.

Figure 7(a) shows the CIE color coordinate (($x$, $y$) = (0.17, 0.24)) for the host ($Ba_{1.3}Ca_{0.7}SiO_4$), whereas Figure 7(b) shows the corresponding CIE coordinates (($x$, $y$) = (0.27, 0.33), (0.29, 0.34), (0.30, 0.33), (0.29, 0.34), and (0.31, 0.35)) for the $Dy^{3+}$-doped silicate phosphors $Ba_{1.3}Ca_{0.7-x}SiO_4{:}xDy^{3+}$ when $x$ is 0.01, 0.02, 0.03, 0.04, and 0.05, respectively. As shown in Figure 7(a), the color for the host falls in the blue space. In contrast, the color for the doped samples takes the position of the white region (Figure 7(b)). Here, the intensity ratio of yellow to blue ($I_Y/I_B$) was varied in the range of 0.54–0.68 when the dopant amounts were changed. This hypersensitive phenomenon results in the shift of CIE chromaticity coordinates to the vicinity of the white point ($x = 0.33$, $y = 0.33$). Hence, by manipulating the $Dy^{3+}$ doping percentage in the silicate host, the emission color is tunable from blue to white, presenting the importance of doping engineering.

Finally, Figure 8 shows the PL decay curves for the silicate phosphors, $Ba_{1.3}Ca_{0.7-x}SiO_4{:}xDy^{3+}$ ($x = 0.00$, 0.01, 0.02, 0.03, 0.04, and 0.05). The decay curves were fitted using the second-order exponential equation [59, 60].

$$I(t) = I_0 + A_1 \exp\left(-\frac{t}{\tau_1}\right) + A_2 \exp\left(-\frac{t}{\tau_2}\right), \quad (3)$$

where $I(t)$ is the time ($t$)-dependent intensity, $I_0$, $A_1$, and $A_2$ are the three constants, and $\tau_1$ and $\tau_2$ are the decay times. The average lifetime $\langle\tau\rangle$ is defined as $(A_1\tau_1^2 + A_2\tau_2^2)/(A_1\tau_1 + A_2\tau_2)$. Resultantly, the decay parameters are given in Table 3, based on the PL curve fitting. As shown in Figure 8, the 3 mol% $Dy^{3+}$-doped silicate phosphor ($Ba_{1.3}Ca_{0.7-x}SiO_4{:}xDy^{3+}$ ($x = 0.03$)) showed both longer lifetime and lower decay rate (see the blue solid line). The longest average lifetime $\langle\tau\rangle$ is 2.12 ms when $Dy^{3+}$ ions were 3 mol %, confirming again that the "3 mol% of $Dy^{3+}$ ions" should be the optimum condition in line with the PL data.

## 4. Conclusion

Single-phase silicate phosphors $Ba_{1.3}Ca_{0.7-x}SiO_4{:}xDy^{3+}$ doped with $Dy^{3+}$ ions ($x = 0.01$, 0.02, 0.03, 0.04, and 0.05) were well prepared using a gel-combustion method. Then, the structural, morphological, and optical properties were characterized in detail. XRD data confirm that the silicate phosphors have a hexagonal unit cell. However, when the host was doped with $Dy^{3+}$ ions, the $d$-spacing was reduced from 0.291 nm (host) to $0.288 \pm 0.001$ nm (doped), indicating the enhanced interactions between the (110) crystallographic planes. Furthermore, the optical bandgap was also reduced from 3.85 eV (host) to $3.74 \pm 0.09$ eV (doped), which is in line with the XRD data. Morphological analysis showed that the doped samples exhibited more aggregated domains with connectivity and micropores depending on composition. Then, the PL spectra were characterized, confirming that the optimized doping condition is 3 mol % $Dy^{3+}$ ions for the silicate ($Ba_{1.3}Ca_{0.7}SiO_4$) phosphor. Finally, the CIE coordinates fall into a white space based on the combined emission of blue, yellow, and red electromagnetic waves. Therefore, the dysprosium-doped silicate phosphors are well applicable to WLEDs for SSL and display devices.

## Data Availability

The data used to support this study are included within the article.

## Conflicts of Interest

The authors declare that they have no conflicts of interest.

## Acknowledgments

This work was supported by both Jimma University in Ethiopia and University of the Free State in South Africa.

## References

[1] H. A. Höppe, "Recent developments in the field of inorganic phosphors," *Angewandte Chemie International Edition*, vol. 48, no. 20, pp. 3572–3582, 2009.

[2] S. Ye, F. Xiao, Y. Pan, Y. Y. Ma, and Q. Y. Zhang, "Phosphors in phosphor-converted white light-emitting diodes: recent advances in materials, techniques and properties," *Materials Science and Engineering: R: Reports*, vol. 71, pp. 1–34, 2010.

[3] X. Qin, X. Liu, W. Huang, M. Bettinelli, and X. Liu, "Lanthanide-Activated phosphors based on 4f-5d optical transitions: theoretical and experimental aspects," *Chemical Reviews*, vol. 117, no. 5, pp. 4488–4527, 2017.

[4] J. Qiao and Z. Xia, "Design principles for achieving red emission in $Eu^{2+}/Eu^{3+}$ doped inorganic solids," *Journal of Applied Physics*, vol. 129, no. 20, Article ID 200903, 2021.

[5] N. Holonyak and S. F. Bevacqua, "Coherent (visible) light emission from $Ga(As_{1-x}P_x)$ junctions," *Applied Physics Letters*, vol. 1, no. 4, pp. 82-83, 1962.

[6] S. Nakamura, T. Mukai, and M. Senoh, "Candela-class high-brightness InGaN/AlGaN double-heterostructure blue-light emitting diodes," *Applied Physics Letters*, vol. 64, no. 13, pp. 1687–1689, 1994.

[7] S. Nakamura, M. Senoh, N. Iwasa, S. I. Nagahama, and T. Yamada, "Superbright green InGaN single-quantum-well-structure light-emitting diodes," *Japanese Journal of Applied Physics*, vol. 34, no. 10B, pp. L1332–L1335, 1995.

[8] D. A. Steigerwald, J. C. Bhat, D. Collins et al., "Illumination with solid state lighting technology," *IEEE Journal of Selected Topics in Quantum Electronics*, vol. 8, no. 2, pp. 310–320, 2002.

[9] J. K. Sheu, S. J. Chang, C. H. Kuo et al., "White-light emission from near UV InGaN–GaN LED chip precoated with blue/green/red phosphors," *IEEE Photonics Technology Letters*, vol. 15, no. 1, pp. 18–20, 2003.

[10] R. Mueller-Mach, G. Mueller, M. R. Krames et al., "Highly efficient all-nitride phosphor-converted white light emitting diode," *Physica Status Solidi (A)*, vol. 202, no. 9, pp. 1727–1732, 2005.

[11] P. F. Smet, K. Korthout, J. E. Van Haecke, and D. Poelman, "Using rare earth doped thiosilicate phosphors in white light emitting LEDs: towards low colour temperature and high colour rendering," *Materials Science and Engineering: B*, vol. 146, no. 1-3, pp. 264–268, 2008.

[12] A. Sandhu, "The future of ultraviolet LEDs," *Nature Photonics*, vol. 1, p. 38, 2007.

[13] C.-K. Chang and T. M. Chen, "White light generation under violet-blue excitation from tunable green-to-red emitting $Ca_2MgSi_2O_7$:Eu,Mn through energy transfer," *Applied Physics Letters*, vol. 90, no. 16, Article ID 161901, 2007.

[14] J. S. Kim, P. E. Jeon, J. C. Choi, H. L. Park, S. I. Mho, and G. C. Kim, "Warm-white-light emitting diode utilizing a single-phase full-color $Ba_3MgSi_2O_8$:$Eu^{2+}$, $Mn^{2+}$ phosphor," *Applied Physics Letters*, vol. 84, no. 15, pp. 2931–2933, 2004.

[15] W.-J. Yang, L. Luo, T.-M. Chen, and N.-S. Wang, "Luminescence and energy transfer of Eu- and Mn-coactivated $CaAl_2Si_2O_8$ as a potential phosphor for white-light UVLED," *Chemistry of Materials*, vol. 17, no. 15, pp. 3883–3888, 2005.

[16] Z. Jia and M. Xia, "Blue-green tunable color of $Ce^{3+}$/$Tb^{3+}$ coactivated $NaBa_3La_3Si_6O_{20}$ phosphor via energy transfer," *Scientific Reports*, vol. 6, no. 1, Article ID 33283, 2016.

[17] H. Liu, L. Liao, M. S. Molokeev, Q. Guo, Y. Zhang, and L. Mei, "A novel single-phase white light emitting phosphor $Ca_9La(PO_4)_5(SiO_4)F_2$:$Dy^{3+}$: synthesis, crystal structure and luminescence properties," *RSC Advances*, vol. 6, no. 29, pp. 24577–24583, 2016.

[18] V. Kumar, M. Manhas, A. K. Bedyal, and H. C. Swart, "Synthesis, spectral and surface investigation of novel $CaMgB_2O_5$:$Dy^{3+}$ nanophosphor for UV based white LEDs," *Materials Research Bulletin*, vol. 91, pp. 140–147, 2017.

[19] S. Liu, J. He, Z. Wu, J. H. Jeong, B. Deng, and R. Yu, "Preparation and study on the spectral properties of garnet-type $Li_3Gd_3Te_2O_{12}$:$Dy^{3+}$ single-phase full-color phosphor," *Journal of Luminescence*, vol. 200, pp. 164–168, 2018.

[20] R. Nagaraj, V. Rajagopal, A. Raja, and S. Ranjith, "Influence of $Dy^{3+}$ ion concentration on photoluminescence and energy transfer mechanism of promising $KBaScSi_3O_9$ phosphors for warm white LEDs," *Spectrochimica Acta Part A: Molecular and Biomolecular Spectroscopy*, vol. 264, Article ID 120212, 2022.

[21] M. Sheoran, P. Sehrawat, N. Kumari, M. Kumar, and R. K. Malik, "Fabrication and photoluminescent features of cool-white light emanating $Dy^{3+}$ doped $Ba_5Zn_4Gd_8O_{21}$ nanophosphors for near UV-excited pc-WLEDs," *Chemical Physics Impact*, vol. 4, Article ID 100063, 2022.

[22] J. Li, W. Wang, B. Liu, G. Duan, and Z. Liu, "Enhanced $Dy^{3+}$ white emission via energy transfer in spherical $(Lu,Gd)_3Al_5O_{12}$ garnet phosphors," *Scientific Reports*, vol. 10, no. 1, p. 2285, 2020.

[23] P. Sehrawat, A. Khatkar, P. Boora et al., "Emanating cool white light emission from novel down-converted $SrLaAlO_4$:$Dy^{3+}$ nanophosphors for advanced optoelectronic applications," *Ceramics International*, vol. 46, no. 10, pp. 16274–16284, 2020.

[24] Y. Dai, S. Yang, Y. Shan et al., "Single-composition white light emission from $Dy^{3+}$doped," *$Sr_2CaWO_6$ Materials*, vol. 12, no. 3, p. 431, 2019.

[25] P. Sehrawat, A. Khatkar, S. Devi et al., "An effective emission of characteristic cool white light from $Dy^{3+}$ doped perovskite type $SrLa_2Al_2O_7$ nanophosphors in single-phase pc WLEDs," *Chemical Physics Letters*, vol. 737, Article ID 136842, 2019.

[26] B. C. Jamalaiah and Y. Ramesh Babu, "Near UV excited $SrAl_2O_4$:$Dy^{3+}$ phosphors for white LED applications," *Materials Chemistry and Physics*, vol. 211, pp. 181–191, 2018.

[27] P. Dewangan, D. P. Bisen, N. Brahme, and S. Sharma, "Structural characterization and luminescence properties of $Dy^{3+}$ doped $Ca_3MgSi_2O_8$ phosphors," *Journal of Alloys and Compounds*, vol. 777, pp. 423–433, 2019.

[28] P. P. Pawar, S. R. Munishwar, and R. S. Gedam, "Intense white light luminescent $Dy^{3+}$ doped lithium borate glasses for W-LED: a correlation between physical, thermal, structural and optical properties," *Solid State Sciences*, vol. 64, pp. 41–50, 2017.

[29] Y.-C. Lin, M. Karlsson, and M. Bettinelli, "Inorganic phosphor materials for lighting," *Topics in Current Chemistry*, vol. 374, no. 2, p. 21, 2016.

[30] B. Liu, L. Kong, and C. Shi, "White-light long-lasting phosphor $Sr_2MgSi_2O_7$:$Dy^{3+}$," *Journal of Luminescence*, vol. 122-123, pp. 121–124, 2007.

[31] L. Lin, Z. Zhao, W. Zhang, Z. Zheng, and M. Yin, "Photoluminescence properties and thermo-luminescence curve analysis of a new white long-lasting phosphor: $Ca_2MgSi_2O_7$:$Dy^{3+}$," *Journal of Rare Earths*, vol. 27, no. 5, pp. 749–752, 2009.

[32] W. Pan, G. Ning, X. Zhang, J. Wang, Y. Lin, and J. Ye, "Enhanced luminescent properties of long-persistent $Sr_2MgSi_2O_7$:$Eu^{2+}$,$Dy^{3+}$ phosphor prepared by the co-precipitation method," *Journal of Luminescence*, vol. 128, no. 12, pp. 1975–1979, 2008.

[33] Z. Huang, Y.-J. Chen, L. Chen, Y. Xie, L.-J. Xiao, and Y. Yang, "Fluorescence improvement of $Ba_{1.3}Ca_{0.7}SiO_4$ :$Eu^{2+}$,$Mn^{2+}$ phosphors via $Dy^{3+}$ addition and their color-tunable properties," *Ceramics International*, vol. 39, no. 3, pp. 2709–2714, 2013.

[34] M. A. Tshabalala, F. B. Dejene, S. S. Pitale, H. C. Swart, and O. M. Ntwaeaborwa, "Generation of white-light from $Dy^{3+}$ doped $Sr_2SiO_4$ phosphor," *Physica B: Condensed Matter*, vol. 439, pp. 126–129, 2014.

[35] D. Golja and F. Dejene, "Structural and photoluminescence characteristics of the single-host green-light-emitting *T*-phase $Ba_{1.3}Ca_{0.7}SiO_4$: $Tb^{3+}$ phosphors for LEDs," *Chemical Physics Letters*, vol. 741, Article ID 137122, 2020.

[36] D. R. Golja, "Synthesis and characterization of rare-earth doped silicate based nanomaterial for application in light emitting diodes," 2020, https://scholar.ufs.ac.za/bitstream/handle/11660/11269/GoljaDR.pdf.

[37] K. Fukuda, M. Ito, and T. Iwata, "Crystal structure and structural disorder of $(Ba_{0.65}Ca_{0.35})_2SiO_4$," *Journal of Solid State Chemistry*, vol. 180, no. 8, pp. 2305–2309, 2007.

[38] E. E. Snyder, B. W. Buoscio, and J. J. Falke, "Calcium(II) site specificity: effect of size and charge on metal ion binding to an

EF-hand-like site," *Biochemistry*, vol. 29, no. 16, pp. 3937–3943, 1990.

[39] I. Kovrlija, J. Locs, and D. Loca, "Incorporation of barium ions into biomaterials: dangerous liaison or potential revolution?" *Materials*, vol. 14, no. 19, p. 5772, 2021.

[40] J.-Y. Jung, J. Kim, Y.-S. Shim, D. Hwang, and C. S. Son, "Structure and photoluminescence properties of rare-earth (Dy3+, Tb3+, Sm3+)-doped BaWO4 phosphors synthesized via Co-precipitation for anti-counterfeiting," *Materials*, vol. 13, no. 18, p. 4165, 2020.

[41] L. Yang, Z. Mu, S. Zhang et al., "$Dy^{3+}$ Doped $Ca_9Gd(PO_4)_7$: a novel single-phase full-color emitting," *Journal of Materials Science: Materials in Electronics*, vol. 29, no. 8, pp. 6548–6555, 2018.

[42] Q. Wang, Z. Mu, L. Yang et al., "The synthesis and the luminescence properties of $Sr_2Ga_3La_{1-x}D_{yx}Ge_3O_{14}$," *Physica B: Condensed Matter*, vol. 530, pp. 258–263, 2018.

[43] K. Somasundaram, K. P. Abhilash, V. Sudarsan, P. Christopher Selvin, and R. M. Kadam, "Defect luminescence and lattice strain in $Mn_{2+}$ doped $ZnGa_2O_4$," *Physica B: Condensed Matter*, vol. 491, pp. 79–83, 2016.

[44] V. D. Mote, Y. Purushotham, and B. N. Dole, "Williamson-Hall analysis in estimation of lattice strain in nanometer-sized ZnO particles," *Journal of Theoretical and Applied Physics*, vol. 6, no. 1, p. 6, 2012.

[45] M. K. Hussen and F. B. Dejene, "Effect of $Cr^{3+}$ doping on structural and optical property of $ZnGa_2O_4$ synthesized by sol gel method," *Optik*, vol. 181, pp. 514–523, 2019.

[46] V. B. Pawade, N. S. Dhoble, and S. J. Dhoble, "Synthesis and characterization of trivalent RE (RE=$Eu^{3+}$, $Dy^{3+}$, $Ce^{3+}$) doped new $Ca_3Al_2Si_3O_{12}$ materials for NUV-wLEDs," *Materials Research Express*, vol. 2, no. 9, Article ID 095501, 2015.

[47] J. H. Nobbs, "Kubelka-munk theory and the prediction of reflectance," *Review of Progress in Coloration and Related Topics*, vol. 15, no. 1, pp. 66–75, 1985.

[48] K. Pavani, J. S. Kumar, T. Sasikala, B. C. Jamalaiah, H. J. Seo, and L. R. Moorthy, "Luminescent characteristics of $Dy^{3+}$ doped strontium magnesium aluminate phosphor for white LEDs," *Materials Chemistry and Physics*, vol. 129, no. 1-2, pp. 292–295, 2011.

[49] E. Pavitra, G. S. R. Raju, Y. H. Ko, and J. S. Yu, "A novel strategy for controllable emissions from $Eu^{3+}$ or $Sm^{3+}$ ions co-doped $SrY_2O_4$:$Tb^{3+}$ phosphors," *Physical Chemistry Chemical Physics*, vol. 14, no. 32, pp. 11296–11307, 2012.

[50] S. Chemingui, M. Ferhi, K. Horchani-Naifer, and M. Férid, "Synthesis and luminescence characteristics of $Dy^{3+}$ doped $KLa(PO_3)_4$," *Journal of Luminescence*, vol. 166, pp. 82–87, 2015.

[51] G. S. Freiria, A. L. Ribeiro, M. Verelst, E. J. Nassar, and L. A. Rocha, "Effect of $Dy^{3+}$ amount on the structural and luminescence properties of $LaNbO_4$:$Dy^{3+}$ phosphor obtained by one-step spray pyrolysis process," *Journal of the Brazilian Chemical Society*, vol. 29, pp. 594–601, 2017.

[52] J. Zhang, Q. Guo, L. Liao et al., "Structure and luminescence properties of $La_6Ba_4(SiO_4)_6F_2$:$Dy^{3+}$ phosphor with apatite structure," *RSC Advances*, vol. 8, no. 68, pp. 38883–38890, 2018.

[53] D. Singh, J. Kaur, N. S. Suryanarayana, R. Shrivastava, and V. Dubey, "Synthesis and luminescent behavior of UV induced $Dy^{3+}$ activated $LaAlO_3$," *Journal of Materials Science: Materials in Electronics*, vol. 28, no. 3, pp. 2462–2470, 2017.

[54] M. P. Hehlen, M. G. Brik, and K. W. Krämer, "50th anniversary of the Judd–Ofelt theory: an experimentalist's view of the formalism and its application," *Journal of Luminescence*, vol. 136, pp. 221–239, 2013.

[55] B. V. Ratnam, M. Jayasimhadri, K. Jang, H. Sueb Lee, S. S. Yi, and J. H. Jeong, "White light emission from $NaCaPO_4$:$Dy^{3+}$ phosphor for ultraviolet-based white light-emitting diodes," *Journal of the American Ceramic Society*, vol. 93, no. 11, pp. 3857–3861, 2010.

[56] S. N. Ogugua, S. K. K. Shaat, H. C. Swart, and O. M. Ntwaeaborwa, "The influence of $Dy^{3+}$ ions concentration and annealing on the properties of $LaGdSiO_5$:$Dy^{3+}$ nanophosphors," *Journal of Luminescence*, vol. 179, pp. 154–164, 2016.

[57] B. Ma, X. Ma, T. Xu, K. Su, and Q. Zhang, "Crystal structure and luminescence properties of a novel single-phase orange-red emitting phosphor $Ca_9La(PO_4)_7$:$Sm^{3+}$," *RSC Advances*, vol. 8, no. 26, pp. 14164–14170, 2018.

[58] X. Zhang, Z. Lu, F. Meng et al., "Luminescence properties of $Ca_3Si_2O_7$: $Dy^{3+}$ phosphor for white light-emitting diodes," *Materials Letters*, vol. 79, pp. 292–295, 2012.

[59] Z. Liu, B. Yang, J. Zou et al., "Enhancement of reliability and thermal stability of $Ca_{0.2}Sr_{2.73}SiO_5$:$0.07Eu^{2+}$ phosphor by completely substitute Ba for Ca in warm LED Application," *Optical Materials*, vol. 86, pp. 155–164, 2018.

[60] B. M. Mothudi, O. M. Ntwaeaborwa, J. R. Botha, and H. C. Swart, "Photoluminescence and phosphorescence properties of $MAl_2O_4$:$Eu^{2+}$,$Dy^{3+}$ (M=Ca, Ba, Sr) phosphors prepared at an initiating combustion temperature of 500°C," *Physica B: Condensed Matter*, vol. 404, no. 22, pp. 4440–4444, 2009.